Spectral Density of Polarimetric Variables Separating Biological Scatterers in the VAD Display

SVETLANA BACHMANN AND DUSAN ZRNIĆ

Cooperative Institute for Mesoscale Meteorological Studies, University of Oklahoma, and NOAA/OAR/National Severe Storms Laboratory, Norman, Oklahoma

ABSTRACT

Echoes in clear air from two types of biological scatterers mixed within the resolution volumes over a large region, observed with S-band dual polarization radar, are presented. This case occurred in the evening of 7 September 2004, at the beginning of the fall migrating season of song birds (passerines). Polarimetric spectral analyses are used for distinguishing birds and insects in multimodal spectra. Spatial continuity of spectral peaks shows clear separation of insect (wind) speeds from bird speeds. Spectral densities of polarimetric variables exhibit vastly different values at speeds corresponding to insects than from those of birds, allowing the separation of the two scatterer types. Therefore, the statistics of the intrinsic polarimetric variables computed from spectral densities are unbiased and closer to the ensemble statistics of the echo type than the ones obtained with standard processing techniques. A novel display of the spectral densities versus azimuth, termed spectral velocity–azimuth display (SVAD), is constructed for easier viewing and interpretation of the velocity field. Analyses of the SVADs reveal the mean velocities and the directions of the two types of scatterers.

1. Introduction

Vertical profiles of wind are routine products on the national network of Doppler radars [e.g., the Weather Surveillance Radar-1988 Doppler (WSR-88D)]. These winds are obtained using analysis of the velocity–azimuth display (VAD) data (Lhermitte and Atlas 1961; Rabin and Zrnić 1980) and are available whenever backscattering is sufficient to produce detectable signals. Throughout much of the United States and during warm seasons such backscattering is provided by insects present in the planetary boundary layer. Microinsects are weak flyers, their deliberate or inadvertent motion is primarily wind driven. Insects ascend to altitudes of several hundred meters above the ground where they ride the airstreams crossing many kilometers in a single flight (Chapman et al. 2004). Other passive wind tracers such as irregularities in refractive index or smoke plumes are also detected, often together with insects. Furthermore, there are active flyers (e.g., birds, bats, etc.) seen by the radar that move at speeds quite dif-

ferent than the wind and thus contaminate the radar products. Obvious among these are nocturnal migrating songbirds (passerines) that lift just after sunset, migrate until dawn, and rest during day hours to avoid predators. Through a good part of spring and fall their strong echoes appear on radar screens. Most of the migratory bird movements occur at altitudes below 3 km with the bulk of action under 900 m (more information available online at www.npwrc.usgs.gov). Bird flight velocities range from 8 to 22 m s^{-1} (Gill 1994). Many insects also migrate at night. Although their speed can be as high as 8.3 m s^{-1} (Riley 1999), typical values are 1 m s^{-1} or less. Thus, insects often behave as quasi-passive wind tracers. It is this property that makes them suitable for wind measurements with Doppler radars. Thus, we submit that lofted insects enhance echoes needed for wind profiling (Achtemeier 1991; Zrnić and Ryzhkov 1998), whereas migrating and wandering birds bias Doppler wind measurements (Wilczak et al. 1995; Zrnić and Ryzhkov 1998).

We examine Doppler spectra and spectral densities of polarimetric variables and explore their potential for separating birds from insects and obtaining winds aloft. This we do by analyzing one case of echoes in the clear-air planetary boundary layer that occurred during the

Corresponding author address: Svetlana M. Bachmann, CIMMS/NSSL, 120 David L. Boren Blvd., Norman, OK 73072.
E-mail: Svetlana.Bachmann@noaa.gov

fall of 2004 at the time of nocturnal bird migration (section 2). We believe that this is the first documentation of widespread echoes caused by the simultaneous presence of birds and nocturnal insects in the resolution volume of weather surveillance radar. Because there was nothing unusual or special on that evening we suspect that the simultaneous presence of insects and migrating birds is rather ubiquitous. There could be, however, seasonal differences. In early spring of bird migration, insects might be less numerous and less mature than in the summer and fall, hence their contribution to radar return would be smaller.

We present spectra in a VAD format that facilitates the visual separation of insect contributions from bird contributions (section 3). In principle the separation could be automated and used on Doppler radars with no polarimetric capability. Spectral density of polarimetric variables presented and analyzed in the VAD format vastly improves the separation of the two species.

2. Data collection and computation of spectral densities

The first part of this section contains a description of data collection including the radar setup and general environmental conditions. This is followed by a brief description of the computations done to obtain the spectral density of polarimetric variables.

a. Radar data and environmental conditions

Time series data were collected with the National Oceanic and Atmospheric Administration/National Severe Storms Laboratory (NOAA/NSSL) research S-band radar (KOUN) on 7 September 2004 between 6 P.M. and 11 P.M. local time (2300 and 0400 UTC). Examination of these data revealed that diurnal insects contributed to the early return and disappeared at sunset. These were followed by nocturnal birds that ascended rapidly from the ground. Nocturnal insects showed up later possibly because their ascent is slow and/or they might have taken off at a later time. Our purpose herein is to analyze data from the time when both nocturnal insects and birds are mixed in the radar resolution volume. Thus, we choose data from 11 p.m. local time (0400 UTC 8 September 2004). Furthermore, we present evidence in polarimetric spectral signatures implying existence of two vastly different scatterer types. And we demonstrate how to separate the contribution of these by using spectral analysis in the VAD domain.

The radar was in dual-polarization mode, simultaneously transmitting and receiving waves of horizontal
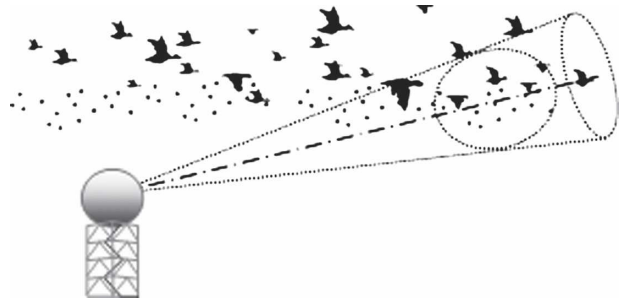

FIG. 1. Simultaneous presence of insects and birds in the radar resolution volume.

and vertical polarizations (Fig. 1). The antenna scanned 360° at elevations of 0.5°, 1.5°, 2.5°, 4°, and 6° with a pulse repetition time (PRT) of 780 μs. The unambiguous range R_a and velocity v_a were 117 km and 35 m s^{-1}, respectively. Samples are spaced 250 m in range, and the depth of the range weighting function (Doviak and Zrnić 1993) is about 300 m. Herein the number of samples M for spectral analysis is 128.

The national network of radars currently uses 17 and 64 samples for the reflectivity and velocity computations, respectively. Smaller M affects the spectral shape by increasing spectral width. Larger M allows better recognition of peaks closely spaced in the velocity space. The radix-2 value is generally chosen for the Fast Fourier Transformation. Obviously 128 samples provides better resolution than 64 samples (~0.5 versus 1 m s^{-1}) but it also requires longer acquisition time. Longer time might not be acceptable for a real-time application; however, it is definitely advantageous in our research application (e.g., for computing the magnitude of the cross-correlation coefficient over closely spaced spectrum coefficients, section 2b).

Spectral moments were obtained and observed in real time on the plan position indicator (PPI) displays while time series data (in phase and quadarature phase components I and Q) were recorded. Spectral processing and analysis of these data are presented herein.

On this day fair weather prevailed over the radar coverage area. At time 0000 UTC and 200 m above ground, a north-northeast wind was blowing at 7 m s^{-1} from 25°; at 800 m it increased to about 11 m s^{-1} and reached a peak of 20 m s^{-1} at the top of the boundary layer (Figs. 2a,b). However, the velocities registered on the PPI are much larger, reaching values up to 30 m s^{-1} (Fig. 3a). The speckled appearance of this field clearly suggests the presence of strong point scatterers. Radar meteorologists recognize this inconsistency and attribute it to "contamination by biological scatterers"; furthermore, they consider such velocities worthless for meteorological interpretation. The purpose of our pa-
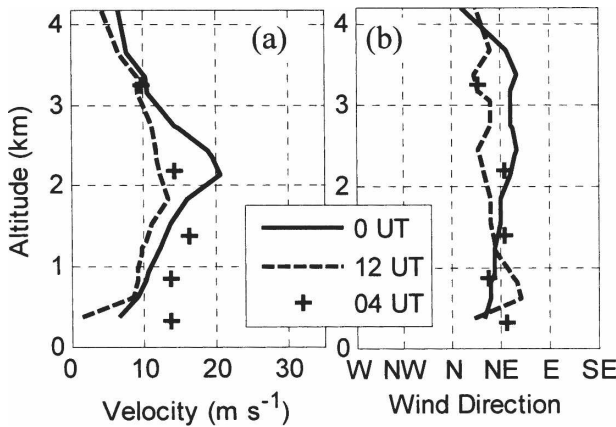
FIG. 2. Vertical sounding of wind from the sounding at 0000 and 1200 UTC 8 Sep 2004: (a) wind speed and (b) wind direction.

per is to demonstrate that spectral analysis and polarimetry can be used to retrieve both the wind and the bird speeds in this and similar situations.

Significant return power is observed in the horizontal (H) and vertical (V) channels through the boundary layer up to about 2 km in height, above which noise dominates. Reflectivity values are relatively low, less than 5 dBZ.

b. Spectral density of polarimetric variables

Doppler spectrum (i.e., spectral density of reflectivity) is computed from the time series data weighted with the von Hann window. There is no universally accepted definition for spectral densities of polarimetric variables. Researchers have defined and used a spectral covariance matrix (Unal and Moisseev 2004), spectral density of differential reflectivity, Z_{DR} (Yanovsky et al. 2005; Kezys et al. 1993), and spectral density of the differential phase (Unal and Moisseev 2004; Kezys et al. 1993). In a dual-polarization system two spectral densities are available; one of signals at H polarization the other at V polarization; from these it is possible to estimate the differential properties at localized resolved Doppler shifts.

For M transmitted pulses there are M spectral coefficients in the spectra from a resolution volume. Let k be an ordered number of spectral (Fourier) coefficient that takes values from 1 to M; k can be transformed to its corresponding radial velocity in the unambiguous velocity interval from $-v_a$ to v_a. Then, $s_h(k)$ and $s_v(k)$ are an H–V pair of complex spectral coefficients containing both the signal and the noise from the corresponding channels. To obtain spectral densities of differential reflectivity the Z_{DR} values are computed for every H–V pair of spectral coefficients of the power
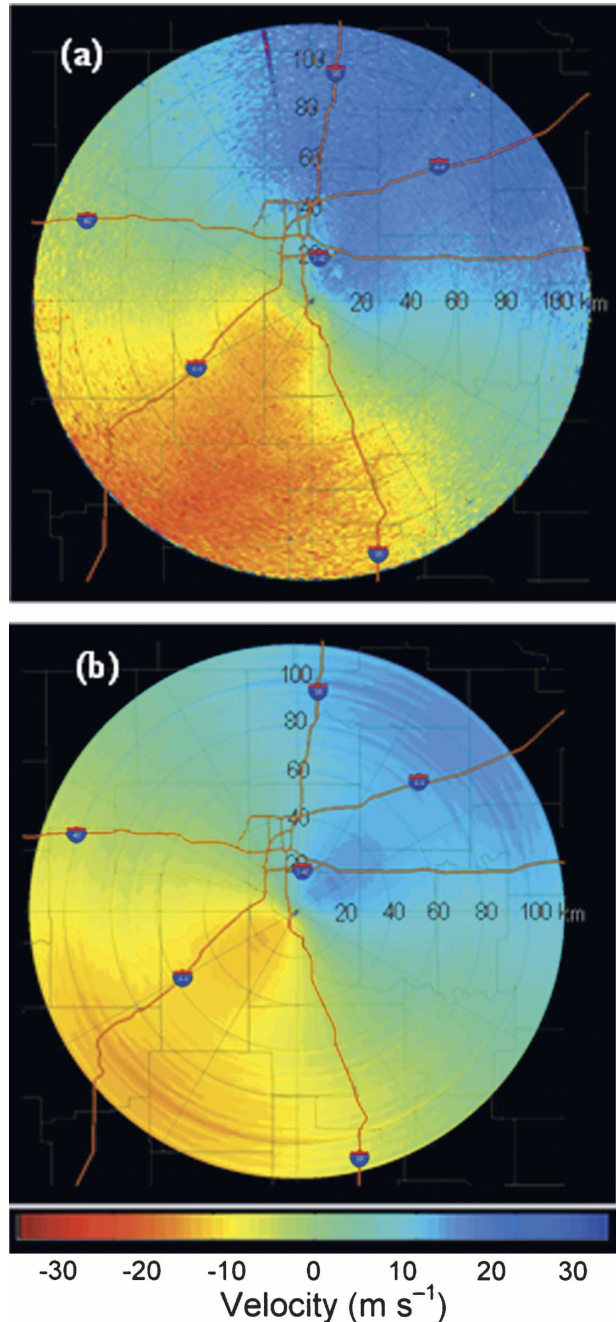

FIG. 3. Velocity fields from H polarization; elevation is 0.5°. The wind direction is NNE, the unambiguous range, $R_a = 117$ km, and the unambiguous velocity, $v_a = 35$ m s^{-1}. The color bar indicates velocity in m s^{-1} and negative values are toward the radar. (a) The field is obtained from the mean velocities. (b) The field is obtained from the SVAD analysis.

spectral densities (Kezys et al. 1993; Yanovsky et al. 2005; Bachmann and Zrnić 2005) according to

$$Z_{DR}(k) = 10 \times \log_{10} \frac{|s_h(k)|^2}{|s_v(k)|^2} + C, \text{ (dB)}, \quad (1)$$
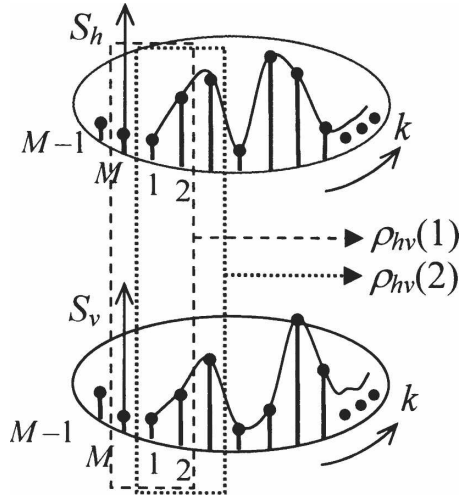
FIG. 4. Three-point running averages on spectral coefficients of H and V channels used to compute ρ_{hv}. To compute $\rho_{hv}(1)$ the Mth, first, and second coefficients enclosed in dashed rectangle are used. Here $\rho_{hv}(2)$ is computed using the first, second, and third coefficients enclosed in the dotted rectangle. In general, $\rho_{hv}(k)$ is computed from $(k - 1)$, k, and $(k + 1)$.

where C is the calibration constant that accounts for the difference in the system gains of the two channels. For the spectral data presented here $C = -2.9$ dB.

Whereas it is possible to define the differential phase as a difference between the phases of the H and V spectral coefficients, one at the time, this is not possible for the magnitude of the correlation coefficient. Thus, we estimate the spectral densities of the complex copolar correlation coefficient (magnitude and phase) from a running three-point average on contiguous complex spectral coefficients of the H and V channels (Fig. 4) as

$$
\rho_{hv}(k) = \frac{\sum_{m=\langle k-1\rangle_M}^{\langle k+1\rangle_M} s_h(m)s_v^*(m)}{\sqrt{\sum_{m=\langle k-1\rangle_M}^{\langle k+1\rangle_M} |s_h(m)|^2 \sum_{m=\langle k-1\rangle_M}^{\langle k+1\rangle_M} |s_v(m)|^2}},
$$
(2)

where $\langle n\rangle_M$ stands for $n \bmod(M)$. The three-point average is chosen to preserve good spectral resolution, comparable to the resolution of the other spectral densities. Maximum spectral resolution could be achieved with a two-point running average, which however would center the spectral estimate in between the adjacent coefficients.

The spectral density of the differential phase Φ_{DP} is computed relative to the system phase SysPhase as

$$
\Phi_{DP}(k) = -\arg(\rho_{hv}) \times 180/\pi + \text{SysPhase}(°). \quad (3)
$$

We estimated the system phase of the KOUN digital receiver from the ground clutter reflectivity returns to be 168°. In the data presented there was no precipitation along the propagation path and the phase in (3) is caused by the differential shift upon backscattering, $\delta(k)$ [i.e., $\delta(k) = \Phi_{DP}(k)$].

3. Data analysis

We start by presenting individual spectra and pointing to the difference between spectral densities corresponding to the two species.

a. Spectra from single-resolution volumes

Because the winds at the time of data collection were north-northeast to south-southwest we choose data from the southern direction to illustrate the separation of these scatterer types in the spectral domain. In that direction the separation of insect and bird velocities in the spectrum is largest (Fig. 5). Velocity values are negative for the scatterers moving toward the radar and positive for the ones moving away.

For example, spectra from the 30- and 40-km range at 0.5° elevation and 180° azimuth (Figs. 5a,b), demonstrate strong peaks at about 8 m s^{-1} evident in both the H (solid line) and V (dashed line) channels. The additional hump at about 20 m s^{-1} in the spectrum from 30 km and horizontally polarized return is better defined than the hump in the spectrum from 40 km. The peaks at lower velocities ($\sim$10 m s^{-1}) are due to insects and the ones at higher velocities are from birds. We deduced this from analyses of atmospheric sounding and the continuity of spectral peaks in the range. The atmospheric sounding indicates calm winds at low elevation (section 2a, Fig. 2a). The continuity of spectral peaks in range is discussed in section 3b. In the spectrum from the 40-km range, the peak at 20 m s^{-1} is bracketed by equally spaced (by 2 m s^{-1}) side peaks. It is unlikely that these peaks are caused by flapping wings. The wing-beat frequency is expected to appear as a pair of side lobes with a modulation shift of wing beat from 0.2 to 0.5 m s^{-1} (5–2 Hz). However, 128 samples do not give enough resolution to observe such small-frequency shifts. A more plausible explanation is that the peaks are produced by birds flying at different speeds.

The medians of power spectra averaged over 5 km exhibit a well-defined bimodal profile (Figs. 5c,d). We present spectral densities of polarimetric variables similarly filtered (medians) over 5 km. This reduces the statistical uncertainty in these densities and is thus pleasant to the eye. For example, spectral density of
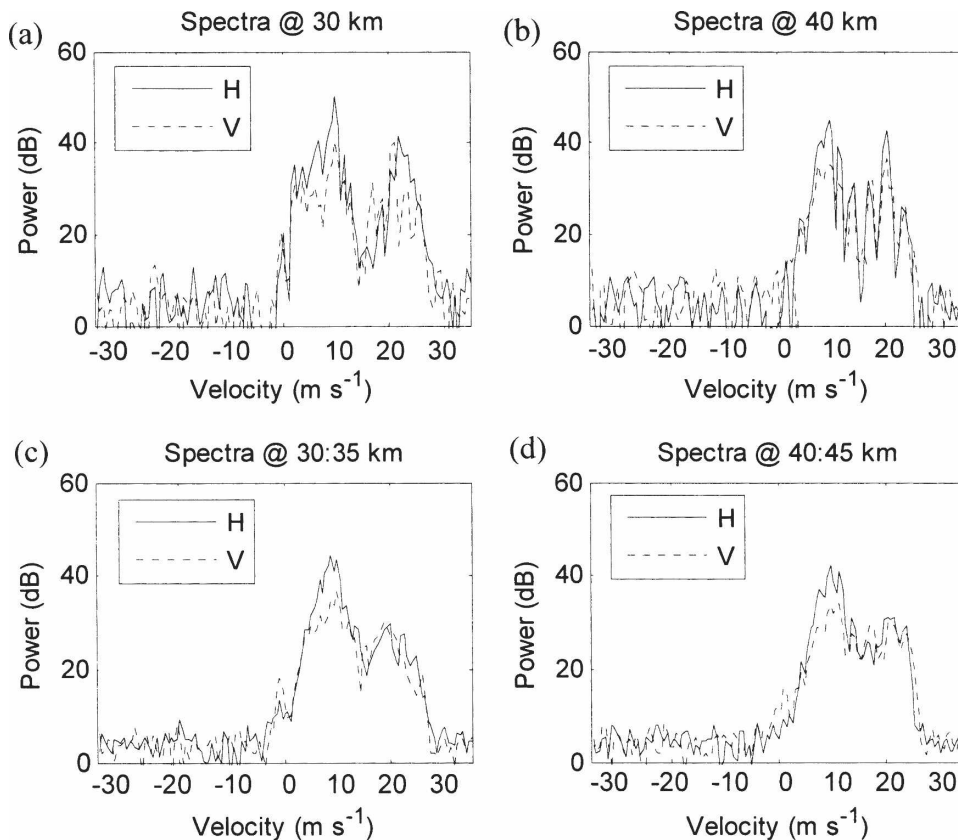
FIG. 5. Power spectrum at azimuth 180°, elevation 0.5°, and range: (a) 30 km, (b) 40 km, (c) median over 5 km from 30 to 35 km, and (d) median over 5 km from 40 to 45 km. The 0 dB on the ordinate corresponds to the noise level. The peaks at about 8 m s^{-1} are caused by insects and the peaks at about 20–22 m s^{-1} are caused by birds.

Z_{DR} (Fig. 6a) at about 8 m s^{-1} exceeds 12 dB, the ρ_{hv} is larger than 0.85 (Fig. 6b), and the backscatter differential phase smoothly changes in the interval 60°–100° (Fig. 6c). These values characterize the returns from insects. At the location of the second spectrum peak (20–22 m s^{-1}), the Z_{DR} is lower and exhibits irregularly rapid changes in the range of −5–15 dB; the ρ_{hv} is below 0.8 (its average is about 0.7), and δ spans the interval −90°–90°. Clearly the polarimetric signatures (Fig. 6) corresponding to the peaks in power (Fig. 5) from insects and birds are quite different.

b. Fields of spectra along the range

Fields of Doppler spectral coefficients are presented as a function of radial velocity and range for easier visual interpretation (Fig. 7a). This format is often used to present Doppler spectra from wind profiling radars (Cornman et al. 1998). The power of the spectral coefficients (in dB-relative units with respect to noise) is color coded. One column in the image at some range R represents the spectrum at that range. In the presence of scatterers the image is expected to display a somewhat continuous distinct color band corresponding to the radial component of the scatterers' velocities. Thus, in an ideal case this band represents the dependence of radial velocities on the range that should be consistent with the sounding wind profile. Other features and blobs, which deviate from the band (path), are contaminants. The appearance and explanation are analogs to the case of wind profiling radars (Cornman et al. 1998), whereby often clear-air spectra are contaminated by birds or ground clutter. The contaminants need to be recognized and filtered to avoid errors in the wind estimates.

Spectral densities of polarimetric variables along the presented radial (azimuth 180° and elevation 0.5°) are in Figs. 7b–d. The field of Doppler spectral coefficients (Fig. 7a) discloses two distinct bands: one continuous (somewhat homogeneous), which stretches along the radial and gradually waves starting at 5 m s^{-1} (near the radar) to 12 m s^{-1} (at 60 km), and even more at larger distance; the other band is sporadic and parallels the
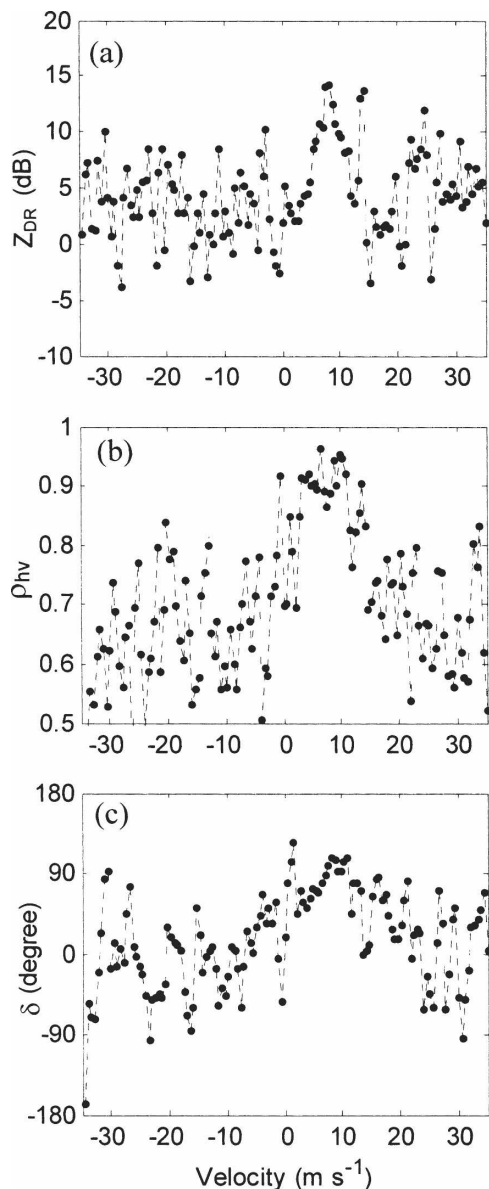
FIG. 6. Spectral densities of polarimetric variables at azimuth 180°, elevation 0.5°; the beginning range is 30 km, and the spectra were obtained from median values over 5 km in range. The stable feature at about 8 m s^{-1} is caused by insects; the ragged feature at about 20 m s^{-1} is caused by birds.

path of the continuous one but with velocities larger by about 10–15 m s^{-1}. The continuous band was observed at all five elevations of the scan and in the same as well as adjacent azimuths. The patchy band is mainly present at low elevations; it breaks into segments and blobs at higher elevations. In the presented radial (Fig. 7a), separation in velocity between the two types of scatterers is very clear. Because of its smoother appearance, lower velocities, and calm winds measured by the atmospheric sounding, we deduce that the continuous

band is caused by wind-blown insects while the patches of the sporadic band are contributions from migrating birds. Apart from one well-defined return at about the 5-km range there are no birds in the beam up to about 10 km. This could be due to the small lateral size of the resolution volume and the fact that the birds fly in a layer. Investigation of polarimetric properties further solidifies the assertion that insects and birds shared the airspace throughout most of the boundary layer on that night.

The two bands evident in the power spectral field (Fig. 7a) have a different appearance in the spectral fields of the polarimetric variables (Figs. 7b–d). Only one band is visible in the spectral densities of Z_{DR}, ρ_{hv}, and δ. This band is caused by insects; it exhibits Z_{DR} values between 3 and 10 dB. The band we attributed to birds appears noiselike in the presented radial. Streaks at ranges of 0–10 km are due to the ground clutter returns and saturation of the receiver immediately following transmission. The copolar correlation coefficient in the insect band appears to be generally larger than 0.7 in the presented radial.

The censored spectral densities (Figs. 8a–d) expose spectral coefficients with significant returns and good copolar correlation and ($S_h > 5$ dB and $\rho_{hv} > 0.7$). The band from birds emerges from noise and exhibits smaller values of Z_{DR} than the one from the insects, and has a larger span of ρ_{hv} values. There are no reports of comparative studies about the differences in ρ_{hv} between insects and birds; rather a threshold of 0.85 is suggested to separate biological scatterers (both insects and birds) from meteorological echoes (Schuur et al. 2003). In the field of spectral differential phase, the measurements due to insects appear as a vivid band with values of about 68°, while a band attributed to birds is "noisy" and spans a large range of δ. The insect band in spectral densities of Z_{DR} and S_h dissipates beyond 70 km due to the small signal-to-noise ratio. However, it is visible in spectral densities of ρ_{hv} and δ and extends to 100 km. The differential phase from insects is almost 30° larger than the value of 40° previously reported by Zrnić and Ryzhkov (1998). We analyzed data collected earlier in the evening (between 2300 and 0400 UTC) and observed azimuthal and time dependence in values of polarimetric spectral densities. We suspect a seasonal dependency as well. The change of spectral densities in time is gradual before sunset and dramatic during and right after sunset. Considering a single azimuth, the spread and the mean value of δ-spectral densities are changing as follows. The spread is relatively small during daytime, decreases before sunset, but exceeds 20 m s^{-1} after sunset and during the night. The mean value is relatively small and gradually
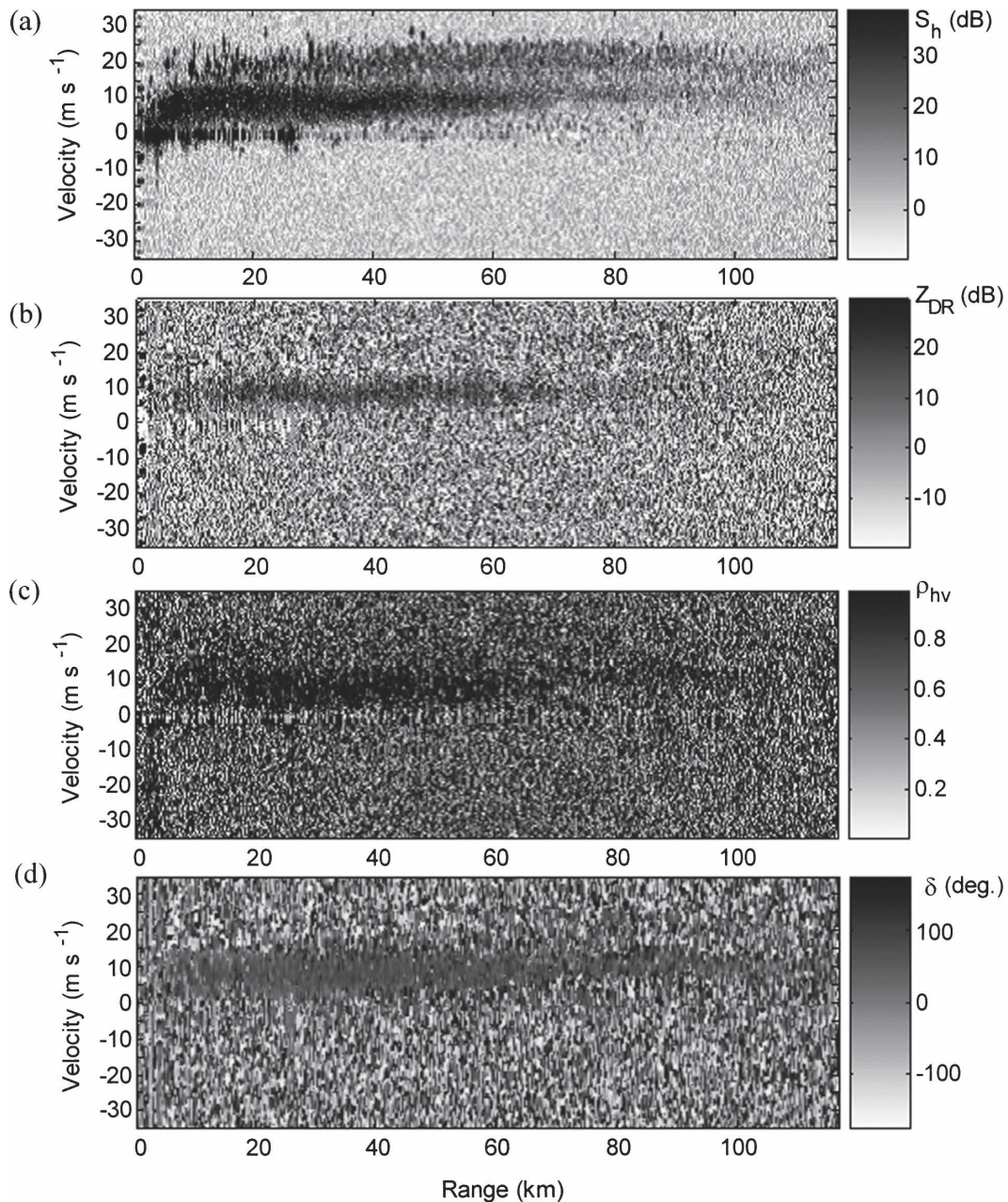
FIG. 7. Spectral densities of power (a) S_h, and polarimetric variables (b) Z_{DR}, (c) ρ_{hv}, and (d) δ. The azimuth is 180° and the elevation is 0.5°.

changes before the sunset and corresponds to diurnal insects (Zrnić and Ryzhkov 1998). At sunset the spread of values is larger and is due to presence of descending diurnal scatterers and ascending nocturnal scatterers, which exhibit different polarimetric properties and a large diversity of radial velocities.

At night δ-spectral densities have more complicated content, exhibiting wider spread for birds then for the insects. Moreover, it appears that the nocturnal insects produce larger mean values of δ-spectral densities then diurnal insects. Further investigation of the dependencies of spectral densities of the differential phase is in progress with the aim to document (i.e., understand) the polarimetric signatures of theses scatterer types. To our knowledge such polarimetric spectral density of clear-air echoes was not previously documented. Nonetheless, our findings are consistent with the reported azimuthal dependence of polarimetric variables (Zhang
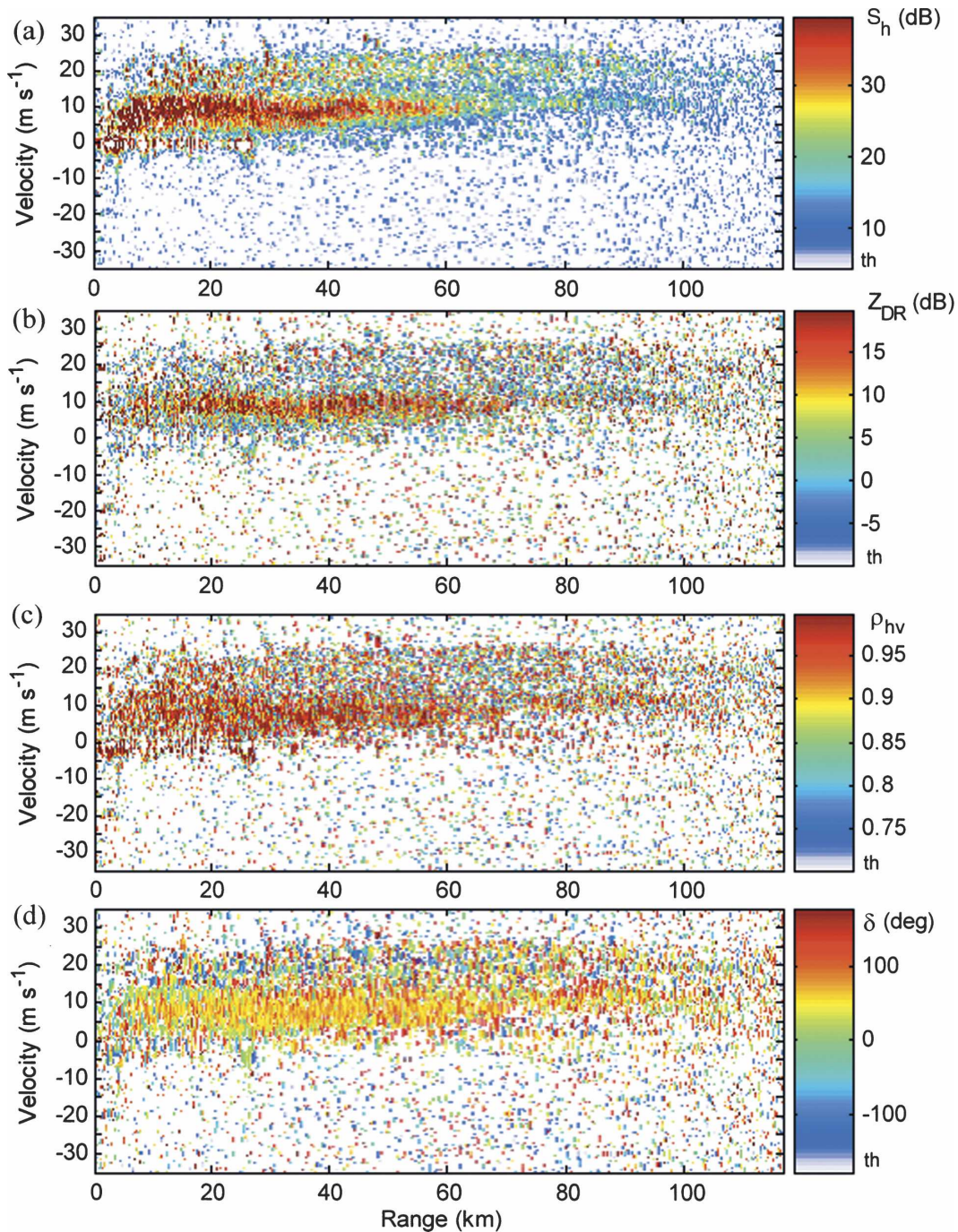
FIG. 8. Censored spectral densities of power (a) S_h, and polarimetric variables (b) Z_{DR}, (c) ρ_{hv}, and (d) δ. The azimuth is 180° and the elevation is 0.5°.

et al. 2005; Zrnić and Ryzhkov 1998), corresponding to the mean densities of the species.

Next we examine the histograms of the polarimetric variables obtained from their spectral densities (Figs. 9a–c). Unbiased Z_{DR} was obtained by subtracting the white noise from the H and V powers whereas bias in ρ_{hv} is insignificant because the SNR threshold of 20 dB above the noise was used. The histograms are computed from the radial at 180° and ranges between 30 and 70 km (Figs. 9a–c). Twelve spectral coefficients centered on a peak corresponding to each species were used in these calculations. The results for insects are
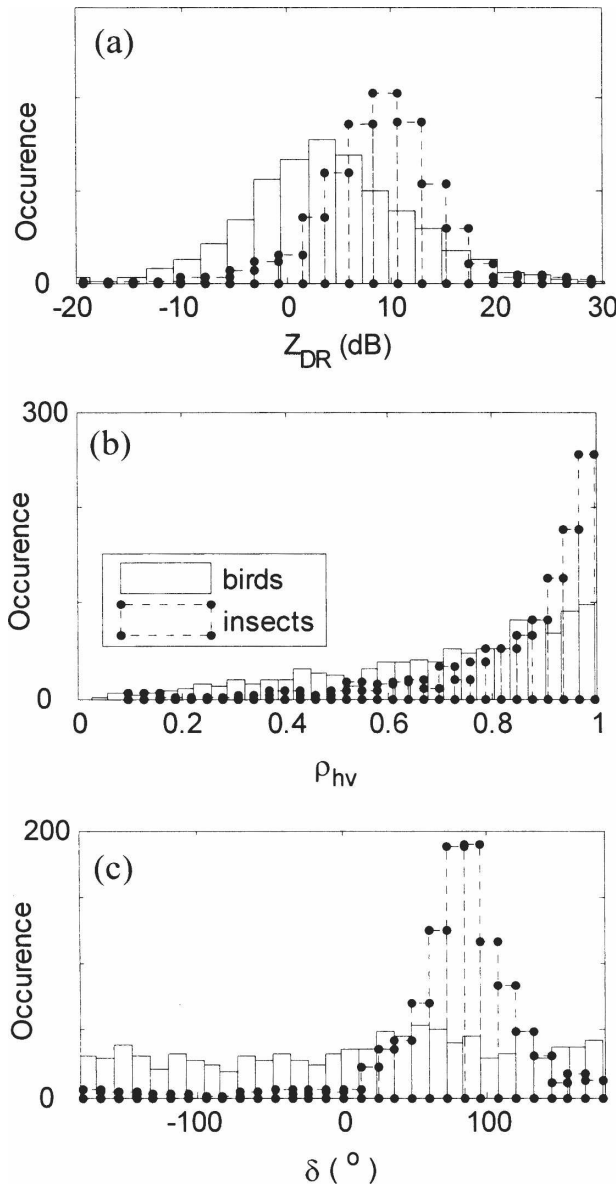
FIG. 9. Histograms of (a) Z_{DR}, (b) ρ_{hv}, and (c) δ along the radial as in Fig. 7, but for data only between a range of 30–70 km are used.

displayed with a dotted line and a dot marker whereas for birds the results are indicated with a solid line. Note the broader distribution of Z_{DR} from the birds and the larger (by 7 dB) mean value for the insects. The distributions of ρ_{hv} from insects and birds intersect at about 0.8, both distributions are skewed, and the one from insects has a significantly larger mean value by about 0.15. Noteworthy is the flat distribution of δ for birds and the concentrated distribution for insects with a crest at about 70°. There is considerable separation in the histograms for this radial that is directed almost along the wind thus enhancing separation in the spec-

trum domain. Even though the histograms of polarimetric spectral fields overlap, the offsets are obvious and the mean values of the distributions differ. Discrimination is more challenging along radials where the two species have less obvious separation in velocity than in the presented radial.

4. Spectral VAD

The VAD technique has been used to determine several features of the wind field: aerial average wind speed, direction, divergence, and deformation. The zeroth harmonic of the VAD provides the horizontal divergence. The first harmonic of the VAD gives the average wind speed and direction (see, e.g., Doviak and Zrnić 1993). The resultant deformation and orientation of the axis of dilatation can be found from the second harmonic. First, we briefly state the impact of the migratory bird movement on the VAD-derived winds, and then we present spectral VAD (SVAD) and use it to eradicate the velocities from migrating birds.

a. VAD contamination issue and a possible solution

The VAD algorithm (Rabin and Zrnić 1980), currently deployed on WSR-88D network, uses the 30-km range as a default slant range for the wind speed and direction computations and one single range location for all azimuths. If there are at least 25 "good" velocity values, the least squares fit is performed and the wind speed and direction from the resulting sinusoidal curve are used to produce a wind barb in the vertical wind profile product. If migrating birds are involved, the good velocity might be heavily biased toward the bird velocities. Automatic recognition of such bias is not available and decontamination would be quite difficult to achieve. Increasing the number of range locations and filtering the deduced VAD velocities does not help if the number of flying birds is large (i.e., if birds are present in neighboring range locations and over a large area).

Power spectral density provides the distribution of velocities within the resolution volume containing both insects and birds. The analysis of the velocity distribution simultaneously with polarimetric properties can associate the correct velocity to the proper species. Furthermore, a median of the distributions from several range locations can reduce contamination because of the sporadic presence of birds (peaks might not be present in every range location, and if present are located at different velocities due to variable pace and intermittent spatial beam filling of the migrating passerines).

b. Fields of spectra in azimuth—VAD spectral representation

Herein we present the spectral densities in the VAD format (i.e., SVAD). The azimuth angle is along the abscissa, the velocities (spectral coefficients) are along the ordinate, and the intensity-coded spectral values are depicted with the gray shades. To construct SVADs we compute spectral fields for all 360° of the scan. Thus, the SVAD technique provides distributions of the polarimetric variables in the azimuth and velocity space.

In Fig. 10a the Doppler spectra are presented in the SVAD format. For vivid visual effect we chose ranges from 30 to 70 km thus avoiding contamination by close ground clutter and noise far from the radar. Each spectral coefficient at a fixed azimuth is a median of 120 spectra (between 30 and 70 km). Two traces are clearly seen and both have sinusoidal shapes. One sinusoid indicates a maximum velocity of about 12 m s^{-1} and a direction from northeast to southwest. The other sinusoid has a maximum of 20 m s^{-1} and a direction from north to south. Although the large averaging interval produces very pleasing plots it comes at a reduced resolution in height. Thus, for obtaining vertical profiles of wind we present (and use) median spectral densities from the range interval of 30–35 km.

In the SVAD of the differential reflectivity (Fig. 10c), the sinusoid with smaller amplitude appears as a well-defined curve and corresponds to the insect returns. The sinusoid with larger amplitude exhibits smaller Z_{DR} values and has discontinuities in the azimuth. This sinusoid is due to returns from birds. At the directions where the two sinusoids intersect, the Z_{DR} from insects dominates. The maxima of differential reflectivity (not shown) as a function of azimuth are between 3 and 8 dB for insects and are less than about 2.5 dB for birds. These are consistent with previous measurements (Zrnić and Ryzhkov 1998). Furthermore, the maximum values for insects occur in the direction of the wind similar to observations by Zhang et al. (2005) who suggest that the strong difference between Z_{DR} along the wind direction and perpendicular to it is caused by the presence of large insects (moths and locusts), which can fly at speeds of 3–5 m s^{-1}.

Both the copolar correlation coefficient and the backscatter differential phase (Figs. 10d,e) well depict the sinusoidal shape corresponding to insect returns. With increasing height the depiction is poorer but visible.

Estimation of insect velocities can be achieved using the SVAD. Application of thresholds on the polarimetric variables in the SVAD can eradicate contributions from scatterers with different polarimetric signatures. In some cases (or aspect angles), diverse scatterers might have similar polarimetric signatures and thus would be hard to separate. Because there are four SVADs (one for each polarimetric variable) it follows that a combined use of these would facilitate better separation of scatterers than what is possible from a single SVAD. The sinusoids in Fig. 10 intersect at about 60° and at 240° challenging separation attempts at these azimuths. Therefore, the velocity values estimated from such SVADs might have gaps. Such gaps are due to uncertainty caused by mixing of the polarimetric values at the intersection of scatterer bands (sinusoids), or by changes associated with different aspect angles. The suitable VAD technique (Rabin and Zrnić 1980) for such data with gaps is part of a suite of algorithms on the WSR-88D. The technique is based on the assumption that the power of higher harmonics can be neglected and the zeroth and first harmonic are obtained from the least squares fit.

Next we apply the procedure to the SVADs from the four elevation angles to obtain the winds (i.e., velocity of insects) as function of height. First, thresholds are applied simultaneously to all polarimetric spectral densities as follows. The adaptive threshold is applied to the field of differential reflectivity to remove all spectral coefficients with Z_{DR} below half the maximum of the median value at the specified velocity bin. All spectral coefficients having the copolar correlation coefficient below 0.7 are discarded. A median filter over three range locations and six spectral coefficients (on each polarimetric spectral density) is applied. All spectral coefficients corresponding to the Z_{DR} values below 2 dB are removed. The largest differential reflectivity previously measured from birds is 2 dB (Zrnić and Ryzhkov 1998). After the thresholds have been applied we take the velocity associated with the maximum of the differential reflectivity in the spectrum at each azimuth and use the least squares fit described by Rabin and Zrnić (1980) to generate the wind speed and direction.

c. VAD from SVAD

The example presented in Fig. 11 shows VADs deduced from SVADs of differential reflectivity at four elevation angles and ranges from 30 to 35 km. The maximum value of Z_{DR} is chosen at every azimuth and the corresponding velocity value is recorded and used in the standard VAD technique. The cross marker indicates the recorded velocities. The solid line shows the estimated velocity from the harmonic least squares fit. From these VADs, the directions and velocities of insects (hence wind) are deduced. Data points derived in this manner are indicated in Fig. 2 with a cross marker. The time of radar measurements is 0400 UTC and the
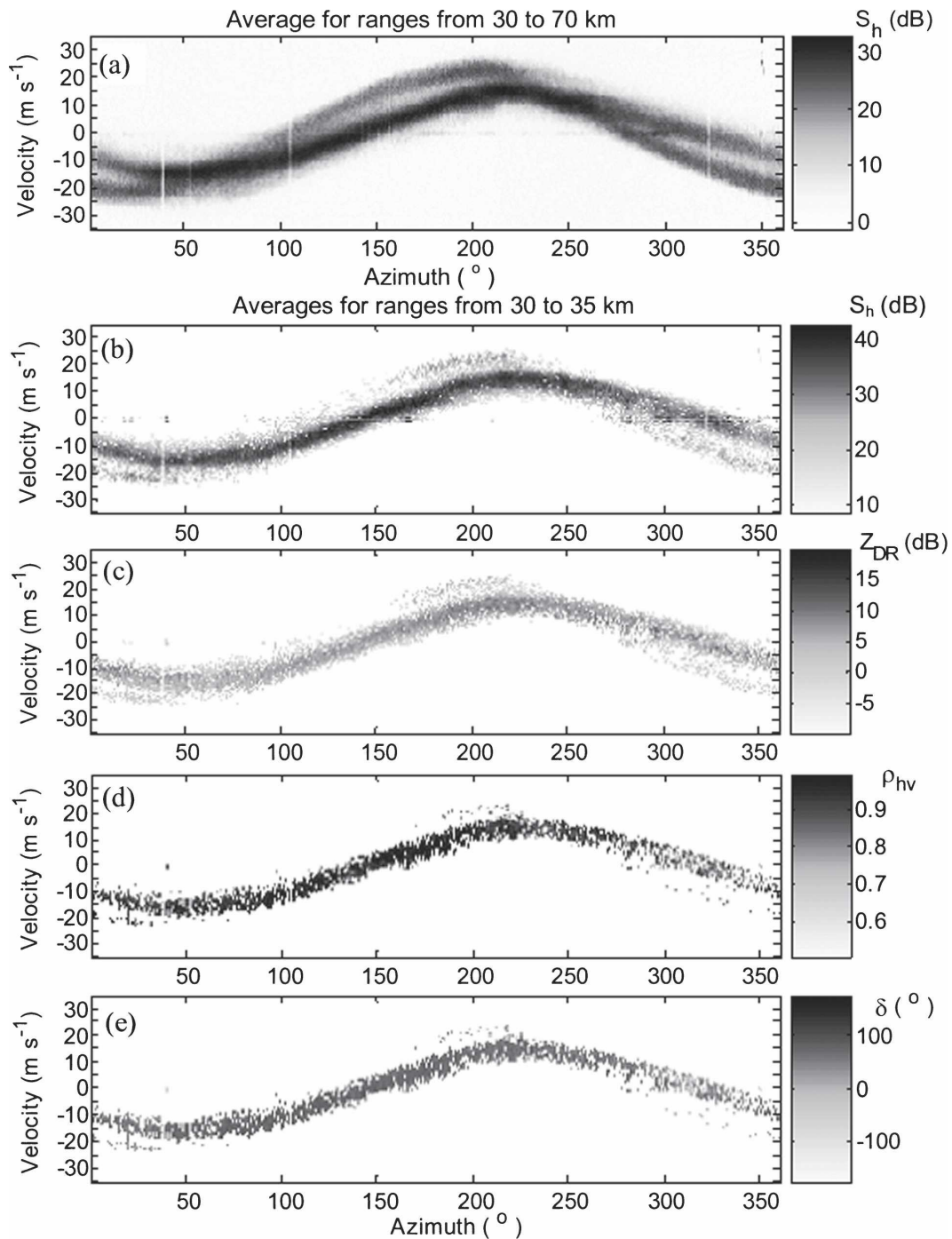
FIG. 10. Spectral VAD: (a) spectra of H polarization power, median values from a range of 30–70 km; (b) spectra of H power, median values over 5 km; (c) Z_{DR} spectra, median over 5 km; (d) ρ_{hv} spectra, median over 5 km; and (e) δ spectra, median over 5 km.

VAD-deduced speeds and directions agree better with the radiosonde observations at 0000 UTC. The difference in wind velocity might be due to the onset of the low-level jet at night or the dominant insects might be active flyers.

The SVAD analysis has been applied to all the data at the 0.5° elevation using the same procedure as for Fig. 11; however, it is a running SVAD incrementing at 250-m intervals and taking a range median on 20 spectra (5 km). The number for averaging is suffi-
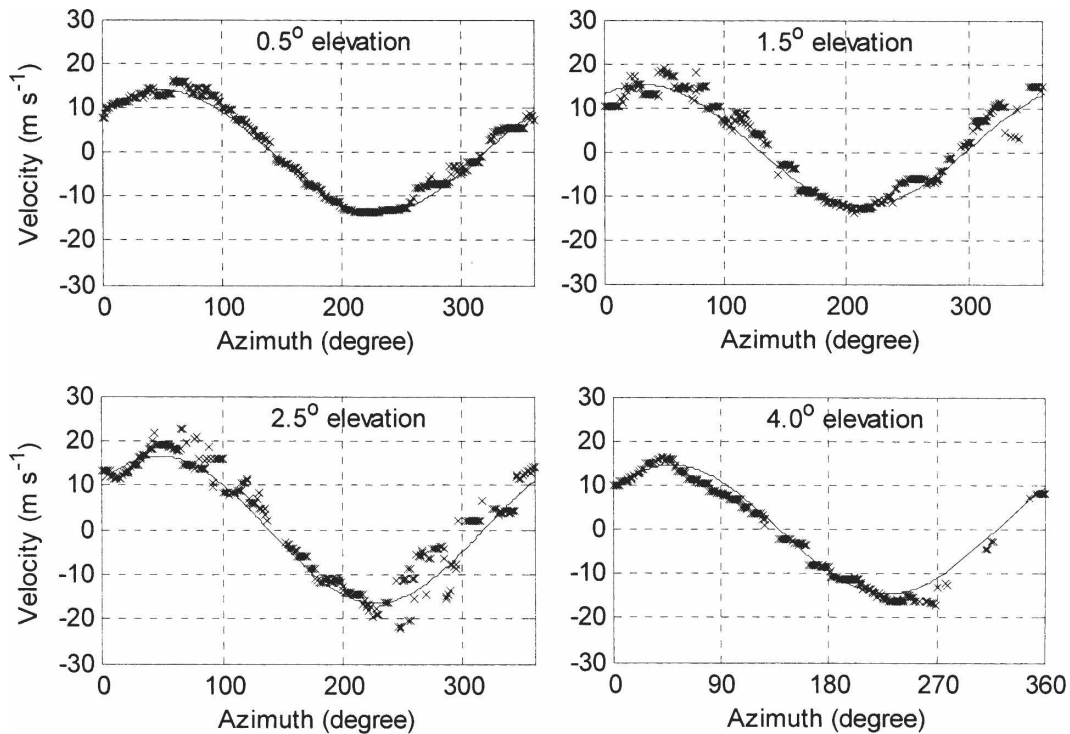
FIG. 11. The VADs obtained from the spectral densities of differential reflectivity. Median values of the spectra of Z_{DR} over a 1-km range interval are used at elevations of 0.5°, 1.5°, 2.5°, and 4°.

cient to reduce the statistical estimate of the median. For an exponential distribution of spectral power coefficients the standard deviation of the median equals $S_h(k)\{\ln(2)/20\}^{1/2}$; where $S_h(k)$ is the true mean. Clearly the reduction in the standard deviation of 5.37 is sufficient to obtain reliable estimates while maintaining sufficient range resolution and allowing only a small increase in altitude along the averaging range interval. The resulting field is depicted in Fig. 3b; it is much smoother than the original and the large velocities are gone. Furthermore, the decrease of velocities between 50 and 80 km is evident and the higher values at closer range hint that a low-level jet might be present.

d. Relative importance of polarimetric parameters

In the mean, the Z_{DR} of wind-tracing insects is larger than that of birds. However, the body shape of the night and day time wind tracers might not be the same. We believe we observed two types of dominant insects: one type was early in the evening and the other was later at night. The Z_{DR} is a sufficient parameter for the SVAD analyses in cases, as presented, when high Z_{DR} is detected in most azimuths. We observed such situations during the night in the fall. However, in our observations insects were more elongated earlier in the evening. Consequently, the displayed Z_{DR} field has a

characteristic, symmetric, and bowlike shape with very high values in the bow and smaller values outside. Moreover, at the azimuths where the Z_{DR} of insects is relatively small the Z_{DR} of birds in some instances exceeded the Z_{DR} of insects. In such (and similar) cases, the Z_{DR} might be ambiguous in discriminating birds and insects.

We observed that the spectral density of differential phase is potentially an excellent discriminator of scatterer types if it is used in coalition with the spectral density of the copolar correlation coefficient. Detailed analyses are deferred for additional studies.

Spectral density of the copolar correlation coefficient is very important because it allows for the censoring of the spectral coefficients exhibiting low cross correlation. This eliminates most of the spectral noise, because the mean spectral of ρ_{hv} computed from three spectral coefficients [Eq. (2)] is 0.43 (Lee et al. 1994).

5. Conclusions

The ubiquitous presence of insects and birds in the Great Plains is routinely observed on weather radar displays. Whereas the former are mostly passive wind tracers, the latter have speeds comparable to, or larger than the environmental wind. Thus, during the bird migration season in spring and fall, standard estimates of

Doppler shifts are contaminated by contributions from bird speeds and therefore are not suitable for meteorological interpretation. Nonetheless, spectral polarimetric analyses identify and discriminate echoes from the two scatterer types.

Spectral analysis of returns in clear air and at night reveals the simultaneous presence of migrating birds and wind-blown insects throughout the boundary layer. The polarimetric variables (e.g., return power, differential reflectivity, copolar correlation coefficient, and differential phase) associated with resolvable Doppler shifts are computed from the Doppler spectra of horizontally and vertically polarized returns. Thus, the spectral density of these polarimetric variables exhibit separation of the two species. We demonstrate that the speed measurements of insects and migrating birds can be resolved by constructing spectral VADs and isolating the insect velocity sinusoid from the additional sinusoids caused by contaminants such as birds. Furthermore, from the combined use of the spectral densities of the polarimetric variables, it might be possible to reconstruct velocity–azimuth display (VAD) profiles of the wind. Specifically we use the copolar correlation coefficient and the signal-to-noise ratio to isolate the spectral values of Z_{DR} that are caused by insects. Then we associate the velocity at the maximum value of such thresholded Z_{DR} spectra with the return from insects and perform a VAD analysis on these velocities.

There are several ways to separate insects from birds in the spectra of the polarimetric variables, including methods applicable to power spectra such as those developed for wind profiling radars (Cornman et al. 1998). Ours is relatively simple and gave credible but biased comparisons of insect winds with soundings.

The possibilities offered by polarimetric spectral analysis are immense and have hardly been explored. More measurements and analysis at different times of day, seasons, and locations are needed to ascertain the full value of this method.

REFERENCES

Achtemeier, G. L., 1991: The use of insects as traces for "clear-air" boundary layer studies by Doppler radar. *J. Atmos. Oceanic Technol.,* **8,** 746–765.

Bachmann, S. M., and D. S. Zrnić, 2005: Spectral polarimetry for identifying and separating mixed biological scatterers. Preprints, *32d Int. Conf. on Radar Meteorology,* Albuquerque, NM, Amer. Meteor. Soc., CD-ROM, P9R-5.

Chapman, J. W., D. R. Reynolds, A. D. Smith, E. T. Smith, and I. P. Woiwod, 2004: An aerial netting study of insects migrating at high altitude over England. *Bull. Entomol. Res.,* **94,** 123–136.

Cornman, L. B., R. K. Goodrich, C. S. Morse, and W. L. Ecklund, 1998: A fuzzy logic method for improved moment estimation from Doppler spectra. *J. Atmos. Oceanic Technol.,* **15,** 1287–1305.

Doviak, R. J., and D. S. Zrnić, 1993: *Doppler Radar and Weather Observations.* Academic Press, 562 pp.

Gill, F. B., 1994: *Ornithology.* Freeman & Cia, 766 pp.

Kezys, V., E. Torlaschi, and S. Haykin, 1993: Potential capabilities of coherent dual polarization X-band radar. Preprints, *26th Int. Conf. on Radar Meteorology,* Norman, OK, Amer. Meteor. Soc., 106–108.

Lee, J. S., K. W. Hoppel, S. A. Mango, and A. R. Miller, 1994: Intensity and phase statistics of multi look polarimetric and interferometric SAR imagery. *IEEE Trans. Geosci. Remote Sens.,* **32,** 1017–1028.

Lhermitte, R. M., and D. Atlas, 1961: Precipitation motion by pulse Doppler radar. *Proc. Ninth Weather Radar Conf.,* Kansas City, MO, Amer. Meteor. Soc., 218–223.

Rabin, R. M., and D. S. Zrnić, 1980: Subsynoptic-scale vertical wind revealed by dual Doppler radar and VAD analysis. *J. Atmos. Sci.,* **37,** 644–654.

Riley, J. R., 1999: Radar returns from insects: Implications for meteorological radars. Preprints, *29th Int. Conf. on Radar Meteorology,* Montreal, QC, Canada, Amer. Meteor. Soc., 390–393.

Schuur, T., A. Ryzhkov, and P. Heinselman, 2003: Observations and classification of echoes with the polarimetric WSR-88D radar. NSSL Rep., NOAA/OAR, Norman, OK, 45 pp.

Unal, C. M. H., and D. N. Moisseev, 2004: Combined Doppler and polarimetric radar measurements: Correction for spectrum aliasing and nonsimultaneous polarimetric measurements. *J. Atmos. Oceanic Technol.,* **21,** 443–456.

Wilczak, J. M., and Coauthors, 1995: Contamination of wind profiler data by migrating birds: Characteristics of corrupted data and potential solutions. *J. Atmos. Oceanic Technol.,* **12,** 449–467.

Yanovsky, F. J., H. W. J. Russchenberg, and C. M. H. Unal, 2005: Retrieval of information about turbulence in rain by using Doppler-polarimetric radar. *IEEE Trans. Microwave Theory Technol.,* **53,** 444–450.

Zhang, P., A. V. Ryzhkov, and D. S. Zrnić, 2005: Observation of insects and birds with a polarimetric prototype of WSR-88D radar. Preprints, *32d Conf. on Radar Meteorology,* Albuquerque, NM, Amer. Meteor. Soc., CD-ROM, 9R6.

Zrnić, D. S., and A. V. Ryzhkov, 1998: Observation of insects and birds with polarimetric radar. *IEEE Trans. Geosci. Remote Sens.,* **36,** 661–668.